

# Diffusing-wave-spectroscopy measurements of viscoelasticity of complex fluids

T. G. Mason

*Department of Chemical Engineering, Johns Hopkins University, Baltimore, Maryland 21218*

Hu Gang

*Exxon Research and Engineering Company, Route 22E, Annandale, New Jersey 08801*

D. A. Weitz

*Department of Physics and Astronomy, University of Pennsylvania, Philadelphia, Pennsylvania 19104*

Received June 7, 1996; revised manuscript received August 19, 1996; accepted August 19, 1996

We present a new use of dynamic light scattering that permits the determination of the viscoelastic behavior of a complex fluid. By describing the motion of a scattering particle in a viscoelastic medium in terms of a generalized Langevin equation with a memory function, we relate the time evolution of its mean-square displacement to the frequency-dependent storage and loss moduli of the medium. The utility of this technique is illustrated through the application of diffusing-wave spectroscopy to probe the viscoelastic behavior of two complex fluids. The properties of a concentrated suspension of colloidal particles interacting as hard spheres are shown to be strongly influenced by the incipient colloidal glass transition, which leads to an extended range of frequencies over which they behave like an elastic solid. Similar elasticity is observed in a compressed emulsion, resulting in this case from the additional interfacial energy of the deformed droplets. In both cases diffusing-wave spectroscopy is used to measure the frequency dependence of the storage and loss moduli, and these results are compared with those from mechanical measurements. Besides providing a purely optical method for measuring mechanical properties, this technique provides new insight into the origin of the viscoelastic behavior. © 1997 Optical Society of America. [S0740-3232(97)01201-5]

## 1. INTRODUCTION

Diffusing-wave spectroscopy (DWS) has greatly enhanced our ability to probe the dynamics of complex fluids. It extends the utility of dynamic light scattering (DLS) to strongly multiply scattering media,<sup>1,2</sup> allowing new physical phenomena to be measured. One of its most significant new features is the ability to probe the dynamics of scatterers at much shorter length scales and correspondingly shorter time scales,<sup>3,4</sup> which cannot otherwise be observed with traditional, singly scattered light. In particular, many complex fluid materials are quite solidlike; thermal fluctuations still cause motion of the scattering particles, but this motion is highly restricted and can be limited to as little as a few nanometers. Nevertheless, the extent of this motion can provide a great deal of information about the properties of the material, as it directly reflects the elastic properties of the complex fluid. In this paper we discuss the use of DWS to measure the elastic properties of a complex fluid and show how it is possible to measure the full frequency-dependent linear viscoelasticity of the scattering medium.<sup>5</sup> Moreover, we show that these measurements are intrinsically related to the time dependence of the mean-square displacement of the scattering particles; this relationship can provide new insight into the underlying origin of the viscoelasticity of the medium. The basic physical principles that underlie

these measurements do not intrinsically rely on the use of multiply scattered light; thus they should be equally applicable to traditional, singly scattered light. However, the use of DWS greatly extends the types of material that can be studied while also extending the range of moduli that can be probed. Thus, through the use of a combination of DWS and DLS, a wide range of materials and moduli can be measured.

This paper is organized as follows: In Section 2, we present a review of the theory that we use to relate the time evolution of the mean-square displacement of a scattering particle to the linear viscoelastic moduli of the surrounding medium. This is followed by examples of the use of this method. Our initial focus is on the behavior of hard spheres near the glass transition. We quantitatively interpret our results in terms of the mode-coupling theory (MCT), illustrating how the light-scattering measurements can provide physical insight into the viscoelastic behavior. Then we discuss the measurement of the elastic modulus of concentrated emulsions; this example shows that the light-scattering results can yield quantitative measurements of the modulus, even in the absence of a detailed interpretation of the scattering. The paper is concluded with a summary of the advantages of this optical technique for measuring the mechanical behavior of complex fluids and a discussion of the range of applicability of the method.

## 2. THEORY

DWS measures the dynamics of strongly scattering samples.<sup>1,2</sup> As with all forms of DLS, the quantity measured is the correlation function of the temporal fluctuations of the scattered light. In its simplest form, the theory for DWS allows the average mean-square displacement of the scattering particles  $\langle \Delta r^2(t) \rangle$  to be determined from the measured correlation function.<sup>6,7</sup> Here we show that one can use the time-dependent mean-square displacement to determine the linear viscoelastic moduli of the medium.<sup>5</sup> We can obtain physical insight into this relationship by considering two limiting cases. In the case of a purely viscous fluid the particles diffuse and the mean-square displacement increases linearly with time, reflecting the self-diffusion of the particle, which provides a direct measure of the viscosity of the fluid,  $\eta$ , through the Stokes–Einstein equation

$$D = \frac{k_B T}{6 \pi a \eta}, \quad (1)$$

where  $a$  is the radius of the particle.<sup>8</sup> In the other limit the material is a purely elastic solid. A good example of the latter condition is an elastic gel, in which thermal fluctuations directly reflect the elastic modulus.<sup>9</sup> These fluctuations can be probed by the motion of a particle attached to the gel. In this case the particle is not ergodic; that is, the time-averaged correlation function is not equivalent to the ensemble-averaged correlation function. Then the amount of decay of correlation function of the particle provides a measure of the elastic constant  $\kappa$ , which we can obtain by equating the thermal energy of the particle with its elastic energy, giving

$$\kappa = \frac{3k_B T}{\langle \Delta r_m^2 \rangle}, \quad (2)$$

where  $\langle \Delta r_m^2 \rangle$  is the maximum mean-square displacement of the probe particle, which is measured by the light scattering. The factor 3 reflects the contribution of a single mode from the equipartition theorem; however, this relation is not exact at the level of these numerical constants.

We can generalize these results by extending the Stokes–Einstein equation to its frequency-dependent form.<sup>10</sup> We accomplish this by beginning with the generalized Langevin equation to describe the motion of a neutrally buoyant particle of mass,  $m$ :

$$m\dot{v}(t) = f_R(t) - \int_0^t dt' \zeta(t-t')v(t'). \quad (3)$$

Here  $v(t)$  is the particle velocity and  $f_R(t)$  is the random force on the particle, which causes the Brownian motion. This force consists of both the contributions of the surrounding fluid and those that are due to any interactions with any other particles or structures in the medium. The force is assumed to be a Gaussian random variable with zero mean and to be completely decoupled from any past velocity. We introduce a memory function,  $\zeta(t)$ , to describe the viscous damping; by allowing the damping to depend on the velocity at all previous times, we allow for a viscoelastic medium, with the possibility of energy's being stored by the elasticity of the medium and being re-

turned at a later time. We can solve this equation by taking the Laplace transform and using the equipartition theorem to obtain the initial value of the velocity:

$$m\langle v(0)v(0) \rangle = m\langle v(t)v(t) \rangle = k_B T. \quad (4)$$

The Laplace transform changes the convolution integral in Eq. (3) to a multiplication, allowing the Laplace transform of the velocity correlation function to be calculated:

$$\langle v(0)\tilde{v}(s) \rangle = \frac{k_B T}{[ms + \tilde{\zeta}(s)]}, \quad (5)$$

where  $s$  is the Laplace frequency and  $\tilde{\zeta}(s)$  is the Laplace transform of the memory function. The first term in the denominator of Eq. (5) reflects the contribution of inertial effects and is negligible, except at the very highest of frequencies; we neglect it for all further discussion. Using the Laplace transform of the mean-square displacement instead of the velocity correlation function, we obtain

$$\tilde{\zeta}(s) = \frac{6k_B T}{s^2 \langle \Delta \tilde{r}^2(s) \rangle}. \quad (6)$$

This is a relationship between the Laplace transforms of the mean-square displacement and the memory function.

To relate the linear viscoelasticity of the complex fluid to the memory function, we use the stress relaxation modulus  $G_r(t)$ , which relates the macroscopic stress  $\tau(t)$  to the strain rate  $\dot{\gamma}(t)$  at previous times:

$$\tau(t) = \int_0^t dt' G_r(t-t')\dot{\gamma}(t'). \quad (7)$$

The magnitude of  $G_r$  is given by the thermodynamic derivative of the stress with respect to the strain, and the time scales are set by the decay of the stress autocorrelation function,  $\langle \tau(0)\tau(t) \rangle$ . By taking the Laplace transform of Eq. (7) we identify the viscoelastic modulus as the coefficient of linearity between the stress and the strain expressed in the frequency domain,  $\tilde{G}(s) = s\bar{G}_r(s)$ . This notation preserves both  $G_r(t)$  and  $\tilde{G}(s)$  in the appropriate units of a modulus, with the recognition that the Laplace transform of  $G_r(t)$  by itself yields units of viscosity. To obtain the linear viscoelastic moduli we assume that the bulk stress relaxation spectrum is the same as that of the local stress relaxation affecting the scattering particle, which is determined by the stress of the surrounding medium exerted on the particle surface. Whereas exact calculation of this spectrum requires detailed knowledge of the full flow field around a moving particle, we can approximate it by its limiting value at zero frequency in a purely viscous fluid. Thus we use the Stokes law and make the assumption that it can be generalized to all frequencies<sup>5</sup>:

$$\tilde{G}_r(s) = \frac{\tilde{\zeta}(s)}{6\pi a}. \quad (8)$$

Equation (8) represents a mean-field assumption, directly connecting macroscopic stress relaxations to microscopic stress relaxations. Combining Eqs. (6) and (8), we obtain the relationship between the macroscopic viscoelastic modulus and the mean-square displacement:

$$\tilde{G}(s) \approx \frac{k_B T}{\pi a s \langle \Delta \tilde{\mathbf{r}}^2(s) \rangle}, \quad (9)$$

which represents a generalized, frequency-dependent form of the Stokes–Einstein relation. It can be recast into a more familiar form by use of the transform of the time-dependent diffusion coefficient, defined as  $D(t) = 1/6 \partial \langle \Delta \mathbf{r}^2(t) \rangle / \partial t$ , and the complex viscosity spectrum,  $\tilde{\eta}(s) = \tilde{G}(s)/s$ . When it is substituted into relation (9), the transformed diffusion coefficient, albeit Laplace transformed, takes the familiar form

$$\tilde{D}(s) = \frac{k_B T}{6 \pi a s \tilde{\eta}(s)}. \quad (10)$$

Equation (10) reduces to the simple Stokes–Einstein equation for freely diffusing particles in a purely viscous molecular fluid.

All our results are obtained in terms of the Laplace frequency  $s$ , which is more convenient because of the integral expression for the memory function in Eq. (3). However, mechanical measurements of the modulus rely on the application of a sinusoidal excitation and on the determination of the in-phase and the out-of-phase responses,  $G'(\omega)$  and  $G''(\omega)$ , respectively. These functions are related by the Kramers–Kronig relations<sup>11</sup> and can be determined from the single real function  $\tilde{G}(s)$  in relation (9). We first calculate the complex shear modulus,  $G^*(\omega)$ , from  $\tilde{G}(s)$ , using analytic continuation and the substitution  $s = i\omega$ . We then take the real and the imaginary parts of  $G^*(\omega)$  to obtain  $G'(\omega)$  and  $G''(\omega)$ , which ensures that the Kramers–Kronig relations are satisfied over the frequency range probed. To do this in practice we use our light-scattering data to determine  $\langle \Delta \mathbf{r}^2(t) \rangle$ ; we calculate the Laplace transform of these data numerically and then calculate  $\tilde{G}(s)$ , using relation (9). These data are then fitted to a continuous functional form in the real variable  $s$ . Finally, we substitute  $s = i\omega$  and take the real and the imaginary parts to obtain the desired  $G'(\omega)$  and  $G''(\omega)$ . Provided that the functional form properly fits the data for  $\tilde{G}(s)$ , no additional error in  $G'(\omega)$  and  $G''(\omega)$  is introduced by analytic continuation. Moreover, the particular functional form chosen for  $\tilde{G}(s)$  does not influence  $G'(\omega)$  and  $G''(\omega)$ , provided that the parameters in the form can be adjusted so that the form fits the data over the measured range. Instead, the main error is introduced by the numerical Laplace transform, because the temporal range of the data for  $\langle \Delta \mathbf{r}^2(t) \rangle$  is limited. However, this error is most pronounced at the bounds of the data and affects only  $\tilde{G}(s)$  only within approximately a decade of the highest and the lowest frequencies. Moreover, the numerical error at the bounds influences principally the weaker of  $G'(\omega)$  and  $G''(\omega)$ , because the deviation leads to greater uncertainty in the phase of  $G^*$  than in its magnitude.

As a result of the viscoelastic behavior of the medium the correlations in the random forces acting on the particles may exist over extended time scales, reflecting the energy storage of the medium and ensuring thermal equilibrium at all times. As a result, the temporal correlation of the random forces becomes<sup>11</sup>

$$\langle f_R(0) f_R(t) \rangle = k_B T \zeta(t). \quad (11)$$

Equation (11) expresses the fluctuation–dissipation theorem for the viscoelastic medium. This relationship provides insight about the physics that underlies this technique; we are using the fluctuation–dissipation theorem to determine the viscoelastic response of the medium. Thus the probe particle is excited thermally, and the relaxation of this excitation reflects the average response of the medium. We follow the relaxation of this response through the mean-square displacement of the particle. The analysis presented above transforms the stochastic response into its individual frequency components, permitting a comparison with more traditional mechanical data. The essence of this technique is the extension of the Stokes–Einstein relationship between the particle diffusion coefficient and the fluid viscosity. In its usual form, it is a zero-frequency relationship; here we assume its validity at all frequencies. Although this is clearly an assumption, as we show below, empirically it seems to be valid.

### 3. EXPERIMENT

We illustrate the application of this method to the study of the rheological behavior of several representative complex fluid samples. We consider in particular two different types of dispersion, each of which exhibits pronounced viscoelasticity when it is concentrated to sufficiently high volume fractions. The two samples are concentrated suspensions of colloidal particles that interact as hard spheres, and concentrated emulsions. The use of the DWS probe of the viscoelasticity allows us to measure the response over a greatly extended frequency range. In addition, the direct relationship between the viscoelastic response and the mean-square displacement provides considerable new insight into the origin of the viscoelasticity.

We used the same arrangement for the experimental measurements of both samples. The beam from an Ar<sup>+</sup>-ion laser operating at a wavelength of 514.5 nm was focused onto one face of a flat cell containing the sample, and the multiply scattered light transmitted through the cell was collected with a single-mode optical fiber with an attached gradient-index lens. The collected light was split into two equal portions with a fiber-optic beam splitter, and each half was directed onto a separate photomultiplier tube. The output of these two tubes was cross correlated to yield the desired autocorrelation function. This scheme virtually eliminated the deleterious effects of after-pulsing in the photomultiplier tubes and reduced the effects of the dead time in the photomultiplier tubes and in the photon-counting electronics. The transport mean free paths,  $l^*$ , which one must know to determine the mean-square displacements from the DWS data,<sup>2</sup> were determined independently from additional measurements of the static transmission of the samples and by comparison with samples whose  $l^*$  was known. For comparison with the light-scattering measurements, the linear viscoelastic moduli were also measured mechanically with a rheometer, with the samples held in a double-walled Couette cell for samples with lower moduli or between a cone and a plate for samples with large moduli.

### A. Hard-Sphere Colloids

Suspensions of colloidal particles interacting as hard spheres have been widely studied as a model system that reflects the essential behavior of suspensions.<sup>12</sup> The major contribution to the viscoelastic behavior of such suspensions is determined by the Peclet number ( $Pe$ ), or the ratio of shear rate to the inverse of the diffusional relaxation time,  $Pe = \dot{\gamma}a^2/D$ , where  $\dot{\gamma}$  is the shear rate,  $a$  is the particle radius, and  $D$  is the short-time self-diffusion coefficient. At low Peclet numbers the particle configuration relaxes to its equilibrium state faster than the applied shear, and the viscoelastic response is that of a purely viscous fluid. By contrast, when the Peclet number is high the particle configuration cannot relax fast enough, permitting energy storage through the change in entropy that is due to the distorted particle configuration. The consequences of this energy storage mechanism, and the resultant viscoelastic properties of hard spheres, have been reported in several studies of colloidal hard spheres.<sup>13,14</sup> The basic scale of the magnitude of the energy density, and hence the modulus, is set by  $k_B T/a^3$ , the entropic energy density in the suspension. However, in addition, colloidal particles undergo several phase transitions in their structure at increasing volume fractions. If they are highly monodisperse, they can become crystals at volume fractions above 0.49.<sup>15</sup> At even higher volume fractions, above  $\sim 0.58$ , they undergo a colloidal glass transition, as crowding of the particle positions prevents the free diffusion of the particles at longer times, making their motion nonergodic.<sup>16,17</sup> Even if they are not sufficiently monodisperse to crystallize, they will still undergo a colloidal glass transition, although the volume fraction may well increase with increasing polydispersity, and the packing becomes more efficient. As a consequence of both of these phase transitions the colloidal particles become solids; thus these phase transitions should also affect their viscoelastic behavior and should lead to a more complex frequency dependence. This behavior has been observed with traditional mechanical measurements.<sup>18</sup> Further study with the light-scattering method will complement these measurements and could provide additional insight into the origin of the behavior, because the technique is a direct probe of the mean-square displacement of the particles.

We study a suspension of silica particles in ethylene glycol; these particles interact as hard spheres.<sup>14</sup> The particle radius is relatively uniform,  $a = 0.21 \mu\text{m}$ , and the volume fraction is  $\phi \approx 0.56$ ; the viscosity of the ethylene glycol is measured as  $\eta_0 = 17 \text{ cP}$  (centipoise) at room temperature. The sample is not index matched, allowing DWS to be used to measure the dynamics. The measured intensity autocorrelation function, normalized by the background, and with the background subtracted, or  $g_2(t) - 1$ , is plotted in Fig. 1. It exhibits an initial decay of approximately two decades, levels off, and then exhibits a final decay several decades in time later. The fact that the correlation function exhibits the final decay at long times means that the sample is ergodic as probed by DWS; we confirmed this by moving the sample and ensuring that the same correlation function was measured at each position. We note that the conditions for a sample to be ergodic with DWS are much less stringent

than with traditional DLS, because of the much greater sensitivity of DWS to motion.<sup>19</sup> The fact that the correlation function levels off after the initial decay reflects the caging effects of neighboring particles on the motion of the probe particle at this high volume fraction, which directly reflects the consequences of the incipient transition from a liquid to a glass and also represents an additional method for storing energy, which should have direct consequences in the viscoelastic response of the suspension.

To observe the viscoelastic behavior from the DWS measurements we first invert the data to obtain the average mean-square displacement of the particles, using the measured value of transport mean free path.<sup>1,2,20</sup> In addition, we make a small correction to account for the fact that the particles are not quite large enough to permit us to ignore completely any collective effects in the scattering.<sup>6,7</sup> DWS probes an average of the scattering over all scattering vectors  $q$ , weighted by  $q^3$ , as a result of

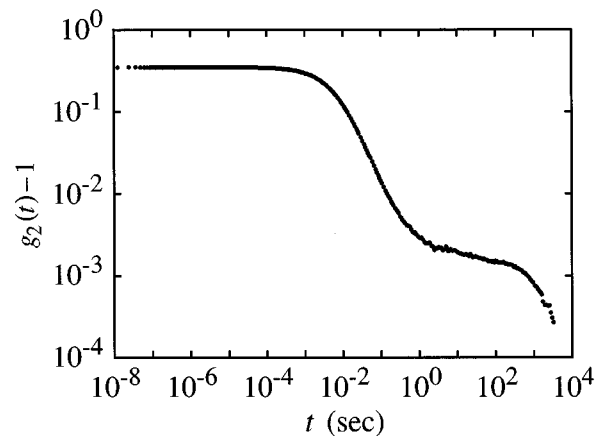


Fig. 1. Temporal dependence of the intensity correlation function  $g_2(t) - 1$  obtained by DWS for a suspension of concentrated silica spheres at  $\phi = 0.56$  with  $a = 0.21 \mu\text{m}$  in ethylene glycol at room temperature. The data have not been normalized for the intercept, which is  $g_2(0) - 1 \approx 0.5$ , as expected for detection of unpolarized light with a single-mode optical fiber.

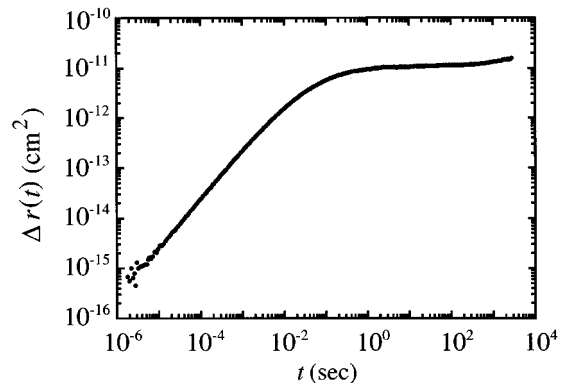


Fig. 2. Temporal dependence of the mean-square displacement for the concentrated suspension of silica spheres. At early times, the linear increase leads to a short-time diffusion coefficient of  $D_s = 4.2 \times 10^{-11} \text{ cm}^2/\text{s}$ .

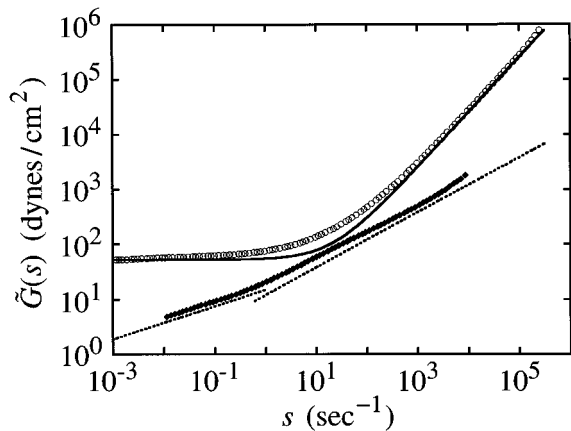


Fig. 3. Frequency dependence of the viscoelastic modulus  $\tilde{G}(s)$  of the concentrated suspension of silica spheres (open circles) and the limiting behavior of a harmonically bound Brownian particle (solid curve). The difference (filled squares) exhibits two power-law regimes (dotted lines), with an exponent of 0.3 at lower frequencies and of  $\sim 0.5$  at higher frequencies.

this weighting the high- $q$  contributions to the scattering dominate the average, and DWS typically probes the self-diffusion of the particles. However, if the particles are small enough, even this weighting is not sufficient to ensure that the average is dominated by the high- $q$  contributions, and there is some contribution of low- $q$  data that reflects collective diffusion. However, the averaging inherent in DWS is well established, and the contributions of the collective effects can be taken into account.<sup>6,7</sup> We account for the contribution of these collective effects by multiplying the data by a  $q$  average of the hydrodynamic interactions,  $h(q)$ , for hard spheres. This procedure results in a correction of a factor of  $\sim 1.5$ , which is applied uniformly to the data and has been shown to account properly for these effects. The results are plotted in Fig. 2, in which we show  $\langle \Delta \mathbf{r}^2(t) \rangle$  as a function of time. The data exhibit an initial linear increase in time, reflecting diffusive motion of the particles at these time scales. The short-time diffusion constant determined from the data is  $D_s = 4.2 \times 10^{-11} \text{ cm}^2/\text{s}$ . At longer times the motion of the particles is highly constrained to an effective saturation displacement of  $r_0 \approx 35 \text{ nm}$ , which is tiny compared with the sphere's radius. The measurement of these small displacements is readily accomplished with DWS. At longer times the interpretation of the DWS data becomes more problematic; the final decay may not reflect the average mean-square displacement of the scattering particles but may instead reflect larger-scale, but more localized and relatively rare, rearrangement events that are reminiscent of those seen in a coarsening foam.<sup>21</sup> Thus we do not extend the inversion of the DWS data to the very longest times.

To determine  $\tilde{G}(s)$ , the modulus as a function of the Laplace frequency, we numerically calculate the Laplace transform of the mean-square displacement and use relation (9). The results are shown in Fig. 3 by the open circles. Below  $s \approx 1 \text{ s}^{-1}$  the viscoelastic modulus exhibits an elastic plateau that depends weakly on frequency. By contrast, at higher frequencies  $\tilde{G}(s)$  crosses over to a

linear behavior, reaching a slope of 1 above  $s \approx 10^3 \text{ s}^{-1}$ . We can obtain some physical intuition about this behavior by considering qualitatively the transformation from Laplace frequency to real frequency. Inasmuch as the substitution results in a phase shift of the frequency by  $90^\circ$ , data that are completely independent of frequency are not shifted and therefore remain real, contributing only to the elastic component of the modulus, or  $G'(\omega)$ . By contrast, data that increase linearly in time are shifted exactly by  $90^\circ$  and thus contribute only to the viscous or loss component,  $G''(\omega)$ . Thus the hard-sphere data at lower frequencies, which are nearly independent of frequency, reflect a dominant elastic component, whereas the data at higher frequencies, which increase nearly linearly with frequency, reflect a dominant viscous component.

We can obtain more-detailed insight into the origin of the behavior by comparing the behavior of  $\tilde{G}(s)$  with that expected for diffusing particles connected to a harmonic spring, which is, on average, unstretched. At short times the elastic force, which is proportional to the particle displacement, is negligible compared with the viscous force, which is linear in the rate of displacement. Thus the mean-square displacement is diffusive. However, at long times, as the particles become increasingly extended from the mean position of the unstretched spring, the elastic force is dominant. On average, thermal energy can excite the particles only to a saturation displacement  $r_0$ , which is determined by the elasticity of the spring. Both short- and long-time behaviors are described by a single equation:  $\langle \Delta \mathbf{r}^2(t) \rangle = r_0^2 [1 - \exp(-t/t_D)]$ , where  $t_D = r_0^2/6D$  is the diffusion time for the confined particle.<sup>9</sup> After taking the Laplace transform of this equation and substituting the result into Eq. (8), we find that

$$\tilde{G}(s) \approx \frac{k_B T}{\pi a r_0^2} (1 + t_D s). \quad (12)$$

The viscoelastic spectrum crosses over from a constant at low frequencies to a linear behavior at high frequencies. By substituting  $s = i\omega$  into relation (12) we identify the storage modulus, or elasticity of the spring, as  $G'(\omega) = k_B T / (\pi a r_0^2) = G_0$  and the loss modulus as  $G''(\omega) = (k_B T / 6\pi a D) \omega = \eta \omega$ , where the viscosity of the fluid obeys the Stokes-Einstein relation. The harmonically bound Brownian particle represents a simple limiting behavior that mimics the basic features of the data and correctly captures the dominant behavior at both low and high frequencies. Thus, to investigate the detailed difference of the observed behavior with this limiting case, we subtract this predicted form from the data. To accomplish this we match the behavior at early and late times by fixing  $\eta = 250 \text{ cP}$  and  $G_0 = 52 \text{ dyn/cm}^2$ . This prediction is shown by the solid curve in Fig. 3, and the difference is shown by the filled circles. The difference can be clearly determined over a large frequency range, indicating that a description in terms of a harmonically bound particle is strictly valid only at the extremes of the frequency range.

The difference exhibits two distinct power laws; below  $s \approx 1 \text{ s}^{-1}$  it behaves like  $\tilde{G}(s) \approx s^{0.3}$ , whereas at higher

frequencies it is more closely described by a different power law,  $\tilde{G}(s) \approx s^{0.5}$ . Dashed lines indicating these exponents are shown in Fig. 3 to illustrate these power-law differences. Each power law covers several decades in frequency and is not sensitive to variations in  $\eta$  and  $G_0$ , provided that the asymptotic behavior of  $\tilde{G}(s)$  is preserved. The existence of these two power laws provides new insight into the physical processes responsible for the behavior observed. The exponent of 0.3 in the modulus is reminiscent of that observed in the glassy dynamics of concentrated hard spheres<sup>17,22</sup> and is consistent with the predictions of the MCT.<sup>23,24</sup> By contrast, the exponent of 0.5 is reminiscent of the behavior predicted for hard-sphere suspensions at high frequencies that are due to a diffusional boundary layer theory.<sup>25,26</sup> Previous experimental evidence for the existence of behavior with this exponent at high frequencies is contradictory. This exponent was observed in mechanical measurements of the elastic modulus,  $G'(\omega)$ , of concentrated hard-sphere suspensions made with a lumped resonator to extend the frequency range.<sup>13</sup> However, measurements made with a traditional shear rheometer, and thus limited to lower frequencies, did not exhibit this behavior when time-temperature superposition was used to extend the effective frequency range; instead, the data were reported to reach a plateau at the highest frequencies.<sup>14</sup> The origin of this discrepancy is not clear; however, one possibility is that lubrication effects become important as the spheres come very close to one another, which is predicted to modify the square root of frequency behavior, causing the data to approach a plateau asymptotically instead.<sup>26</sup>

To compare these results with the more common mechanically measured modulus we must convert from the Laplace frequency to the real frequency,  $\omega$ . We could accomplish this by taking the inverse Laplace transform and then the Fourier transform to obtain the real and the imaginary parts,  $G'(\omega)$  and  $G''(\omega)$ , respectively. Instead, we use analytic continuation; therefore we first find a functional form in  $s$  to describe the data. We can do this by exploiting the physical insight about the system gained from the behavior of  $\tilde{G}(s)$ . Thus we combine the functional forms expected for the contributions for the stress relaxations in a colloidal hard-sphere suspension near the glass transition with the contribution that is due to the diffusional boundary layer and the contribution that is due to the high-frequency viscosity.<sup>18</sup> This provides an explicit functional form:

$$\tilde{G}(s) = G_P + G_\sigma[\Gamma(1 - a')(t_\sigma s)^{a'} - B\Gamma(1 + b') \times (t_\sigma s)^{-b'}] + \sqrt{2}G_D(t_D s)^{1/2} + \eta_\infty s, \quad (13)$$

where  $\Gamma$  represents the gamma function. The first three terms reflect the cage dynamics that account for the plateau and the beginning of the low-frequency, or  $\beta$ , relaxation and are suggested by the MCT.<sup>23,24</sup> In the MCT each particle is considered as being in a cage of neighboring particles in a spatially self-consistent way, thereby coupling the dynamics of differing length scales together. This spatial coupling, in turn, leads to predictions for the average temporal dynamics of the ensemble; these depend on the volume fraction and exhibit the hallmark of the glass transition when they become nonergodic at increas-

ing volume fraction. For the data presented here the correlation function decays at long times, indicating that the particles are ergodic and thus that  $\phi = 0.56$  is on the liquid side of the glass transition. Therefore we use a general asymptotic approximation of the  $\beta$  relaxation for the temporal stress autocorrelation function on the liquid side<sup>22</sup> and then transform this correlation function into the Laplace domain. This results in the first three terms in Eq. (13). We calculate the constants  $a' = 0.3$ ,  $b' = 0.55$ , and  $B = 0.96$  by the MCT by assuming a hard-sphere potential.<sup>17,22,23,27</sup> The fourth term accounts for the predicted high-frequency elastic modulus determined by flow calculations for a diffusional boundary layer,<sup>25,26</sup> where  $G_D = (3/5\pi)(k_B T/a^3)\phi^2 g(2a, \phi)$  and is  $G_D \approx 2$  dyn/cm<sup>2</sup> for our suspension when we use an approximation for the radial distribution function at contact near random close packing,  $g(2a, \phi) \approx 0.78/(0.64 - \phi)$ .<sup>12</sup> The fifth term reflects the high-frequency viscosity of the suspension. The five fitting parameters are the plateau modulus  $G_P$ , which represents the overall scale for the plateau at low  $s$ ; the elastic amplitude scale  $G_\sigma$ , which sets the variation of  $\tilde{G}(s)$  about  $G_P$  at low frequencies; the scaling time  $t_\sigma$ , which determines the inflection point of the MCT contribution; the diffusion time  $t_D = a^2/D_s$ , which is determined by the short-time diffusion coefficient  $D_s$ ; and the high-frequency suspension viscosity  $\eta_\infty$ , which sets the magnitude of the rise in  $\tilde{G}(s)$  for large  $s$ .

The functional form describes the data well. The fitting parameters are  $G_P = 54$  dyn/cm<sup>2</sup>,  $G_\sigma = 3$  dyn/cm<sup>2</sup>,  $t_\sigma = 40$  s,  $t_D = 10$  s, and  $\eta_\infty = 2.5$  P; we use them to determine  $G'(\omega)$  and  $G''(\omega)$ , the real and the imaginary parts of  $\tilde{G}(i\omega)$ , by analytic continuation, setting  $s = i\omega$ . We obtain

$$G'(\omega) = G_P + G_\sigma[u_1(t_\sigma \omega)^{a'} - u_2(t_\sigma \omega)^{-b'}] + G_D(t_D \omega)^{1/2}, \quad (14)$$

$$G''(\omega) = G_\sigma[v_1(t_\sigma \omega)^{a'} + v_2(t_\sigma \omega)^{-b'}] + G_D(t_D \omega)^{1/2} + \eta_\infty \omega, \quad (15)$$

where  $u_1 = \Gamma(1 - a')\cos(\pi a'/2)$ ,  $u_2 = B\Gamma(1 + b') \times \cos(\pi b'/2)$ ,  $v_1 = \Gamma(1 - a')\sin(\pi a'/2)$ , and  $v_2 = B\Gamma(1 + b')\sin(\pi b'/2)$  are constants.

The resultant storage modulus is shown by the solid curve and the loss modulus is shown by the dashed curve in Fig. 4. As expected from the plateau in  $\tilde{G}(s)$ , the storage modulus is dominant at low frequencies; thus, despite the fact that the suspension is still a fluid, it behaves like a solid over an extended range of frequencies. By contrast, at higher frequencies the viscous behavior expected for a fluid becomes dominant, again as expected from the linear rise in  $\tilde{G}(s)$ . The rise in  $G''(\omega)$  toward low frequencies is due to the second (von Schweidler) term in Eq. (15) and results from stress relaxations at long times owing to cage breakup.<sup>24</sup> At high frequencies  $G'(\omega) \sim \omega^{1/2}$ , reflecting the diffusively relaxing stresses given by the fourth term in Eq. (15). We emphasize that these data reflect a purely optical measurement of the shear modulus of the suspension.

To check both the validity of these measurements and the interpretation of the data, we compare these results

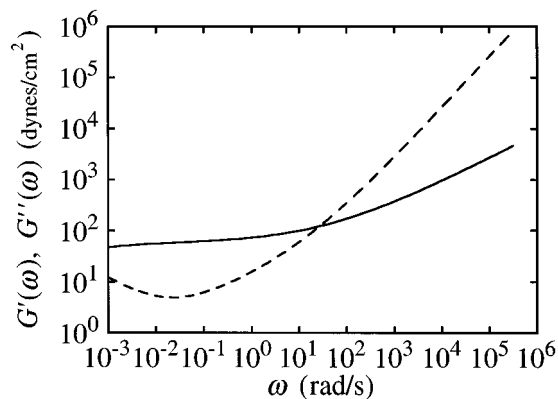


Fig. 4. Storage modulus  $G'(\omega)$  (solid curve) and loss modulus  $G''(\omega)$  (dashed curve), determined optically for the concentrated suspension of silica spheres.

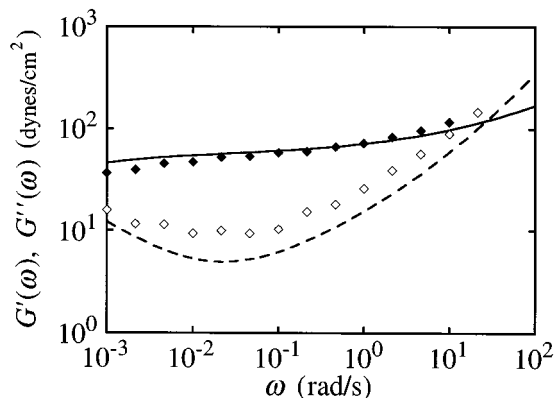


Fig. 5. Comparison of the optical measurements of  $G'(\omega)$  (solid curve) and  $G''(\omega)$  (dashed curve) with mechanical measurements (filled and open symbols, respectively) for the concentrated suspension of silica spheres.

with measurements made with a traditional mechanical rheometer.<sup>1</sup> We employ a controlled strain rheometer, using a double-walled Couette geometry. In Fig. 5 we compare the mechanically measured values of  $G'(\omega)$  and  $G''(\omega)$ , shown by the diamonds, with those obtained optically, shown by the curves. Very good agreement is found, particularly with the storage modulus, which is the larger of the two components. The mechanical measurement of  $G''(\omega)$  is slightly larger than the optical measurement. This may suggest that even the tiny applied mechanical strain  $\gamma \approx 10^{-2}$  may not be completely in the linear regime but may introduce a slight additional convective loss. This result also highlights an important feature of the light-scattering method; because it intrinsically relies on thermal fluctuations, there is no question that the sample remains in thermal equilibrium and that the resultant moduli reflect this.

One of the greatest advantages of the light-scattering technique is the large range of frequencies that it covers. This is immediately apparent from Fig. 5. The traditional mechanical techniques are limited to relatively low frequencies, in our case to  $\omega \leq 10^2$  rad/s. This con-

straint results from the limitations of mechanically oscillating the relatively large mass of the rheometer cell at high frequencies, because of its inertia. By contrast, the probe particle for the light scattering has colloidal dimensions, and thus inertial effects are avoided until much higher frequencies. As a result, the light-scattering data extend to much higher frequencies,  $\omega \approx 10^6$  rad/s.

## B. Emulsions

Emulsions are droplets of one fluid in a second, immiscible fluid, stabilized by a layer of surfactant at the interface. They are similar to the hard spheres in that they are a dispersion of particles in a fluid; they are different from hard spheres in that the particles, being made of fluid, are deformable. The droplets are deformed when they are compressed by an osmotic pressure to volume fractions higher than random close packing,  $\phi_c \approx 0.64$ , the highest volume fraction to which undeformed spheres can be packed. The deformation in their shape leads to a new mechanism for energy storage and hence to an elastic modulus.<sup>28,29</sup> This contribution is due to surface tension, and its scale is set by the Laplace pressure within the spheres,  $\sigma/a$ , where  $\sigma$  is the droplet surface tension and  $a$  is the radius of curvature. The Laplace pressure is the amount of pressure that is necessary to deform the shape of a droplet. Typical emulsion droplets used here are colloidal in scale, with diameters of  $\sim 1 \mu\text{m}$  and with  $\sigma \approx 10$  dyn/cm, giving  $\sigma/a \approx 10^7$  dyn/cm<sup>2</sup>. By comparison, the energy density that characterizes the entropic moduli of hard spheres is  $k_B T/a^3 \approx 10^{-1}$  dyn/cm<sup>2</sup>. Even though this is a lower bound for the moduli for hard spheres, it is so much smaller than the surface-tension contribution that the emulsions have a significantly larger elasticity than the concentrated hard spheres. Thus use of the optical probe of the viscoelasticity requires measuring even smaller displacements, making the use of DWS essential.<sup>10</sup>

We use an emulsion of silicone oil droplets in water, stabilized by sodium dodecyl sulfate. The emulsion is purified by a crystallization fractionation technique<sup>30</sup> to yield monodisperse droplets. The mismatch in the refractive indices of the oil and the water causes these concentrated emulsions to scatter light strongly, permitting the use of DWS. The emulsion is concentrated by centrifugation, and we determine the volume fraction by weighing the emulsion before and after the continuous water phase is evaporated. We measure the correlation function in transmission and determine the transport mean free path from the total transmitted intensity. We use this result to invert the measured correlation function within the theory for DWS to determine the mean-square displacement of each droplet. This interpretation implicitly assumes that the scattered intensity from the emulsion can be determined from the product of a form factor, which reflects the angular dependence of the scattering from isolated droplets, and the structure factor, which reflects the correlations of the droplet positions. Independent measurements<sup>31</sup> of the scattering from monodisperse emulsions, whose continuous phase has been adjusted through the addition of glycerol to index match the oil phase exactly, show that this factorization remains valid even at the high volume fractions studied here. Thus we

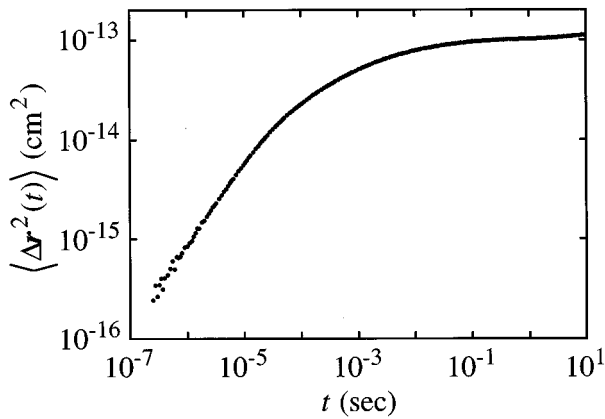


Fig. 6. Temporal dependence of the mean-square displacement of emulsion droplets with  $a = 0.53 \mu\text{m}$  at  $\phi = 0.65$  measured by DWS.

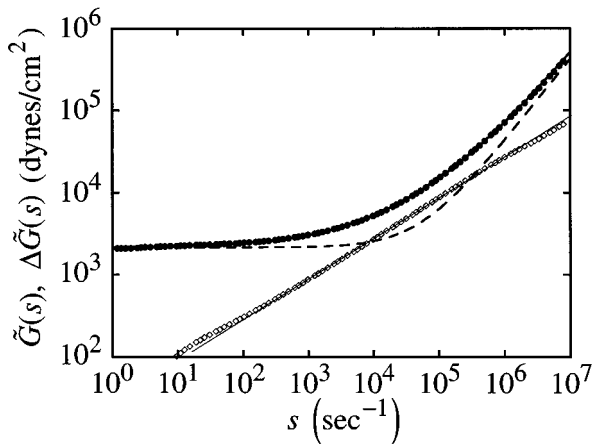


Fig. 7. Frequency dependence of the viscoelastic modulus  $\tilde{G}(s)$  (filled circles) for the concentrated emulsion. The solid curve is a fit to the data and is indistinguishable from the data. The limiting behavior of a harmonically bound Brownian particle is shown by the dashed curve, and the difference (open squares) has an  $s^{0.5}$  frequency dependence, as shown by the solid curve through the data.

assume that the measured dynamics reflect the mean-square displacement of the center of mass of the droplets, recognizing that this is only an approximation.

In Fig. 6 we plot the mean-square displacement of a concentrated emulsion with  $\phi \approx 0.65$  that comprises droplets with a radius of  $a \approx 0.53 \mu\text{m}$ , as determined from DLS from a dilute mixture. The actual volume fraction of oil is  $\phi = 0.62$ , but the stabilizing screened electrostatic repulsion between the droplets, which is due to the ionic surfactant that coats their surfaces; gives rise to an effective packing volume fraction of 0.65 (Ref. 32); this just exceeds random close packing of monodisperse spheres. The measured  $\langle \Delta \mathbf{r}^2(t) \rangle$  is similar in form to that measured for the hard spheres; it rises nearly linearly at short times before saturating at longer times. These data are numerically Laplace transformed, and  $\tilde{G}(s)$  is calculated from Eq. (8); the results are plotted by the filled circles in Fig. 7. The long-time saturation in

$\langle \Delta \mathbf{r}^2(t) \rangle$  leads to a low-frequency plateau in  $\tilde{G}(s)$ , and the early time rise in  $\langle \Delta \mathbf{r}^2(t) \rangle$  leads to a high-frequency rise in  $\tilde{G}(s)$ . To compare these data more explicitly with those of the hard spheres, we again subtract from them the contribution of a harmonically bound Brownian particle matched to the asymptotic limits of the data and shown by the dashed curve in Fig. 7. The difference, shown by the open squares, highlights both the similarity and the difference between the behavior of the emulsions and that of the hard spheres. Rather than being dominated by the two distinct power-law regimes exhibited by the hard spheres, the emulsion data are dominated by a single power law, with an exponent of 1/2.

On the basis of the behavior shown in Fig. 7, we fitted the data for  $\tilde{G}(s)$ , using a functional form that combines the low-frequency constant elasticity, the high-frequency viscous contribution, and the intermediate  $s^{0.5}$  behavior. The fit is shown by the solid curve in Fig. 7 and clearly exhibits very good agreement with the data. We again emphasize that any functional form that describes the data would be equally suitable. Analytic continuation is used to calculate  $G'(\omega)$  and  $G''(\omega)$ , and the results are shown by the solid and the dashed curves, respectively, in Fig. 8. To compare the frequency dependence with the light-scattering data, we measure the elastic moduli by traditional mechanical means, using a strain-controlled rheometer, with the sample contained in a double-walled Couette cell.<sup>32</sup> The frequency-dependent moduli are shown by the symbols in Fig. 8, with filled symbols representing the storage modulus,  $G'(\omega)$ , and open symbols representing the loss modulus,  $G''(\omega)$ . The agreement between the two techniques is excellent. We note again the extended range of frequencies that the light-scattering data cover in comparison with the range covered by the mechanical measurements.

The elasticity of the emulsion increases significantly with increasing volume fraction.<sup>32,33</sup> This is most evident from the rise of the low-frequency elasticity. We can measure this directly by using the light scattering. The leveling off of the correlation function, which leads to

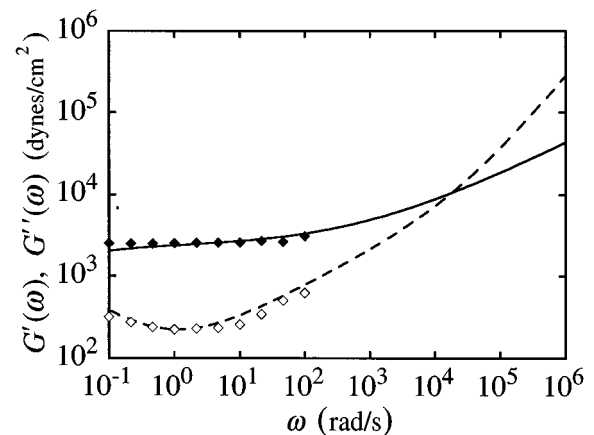


Fig. 8. Frequency dependence of the storage modulus  $G'(\omega)$  (solid curve) and of  $G''(\omega)$  (dashed curve) obtained by analytic continuation of the fit of  $\tilde{G}(s)$  for the concentrated emulsion compared with the mechanical measurements (solid and filled symbols, respectively).

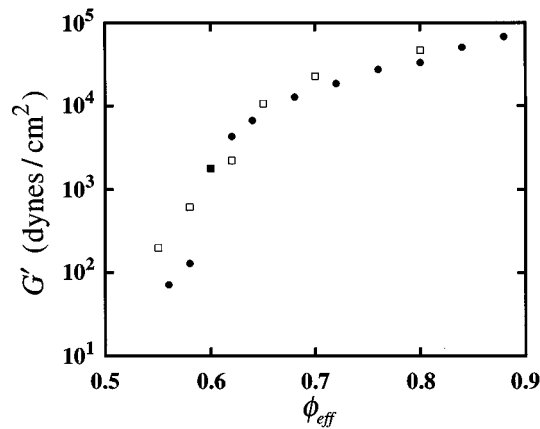


Fig. 9. Comparison of the low-frequency elastic modulus measured mechanically (open symbols) with that measured optically (filled symbols) for a monodisperse emulsion as a function of its effective volume fraction.

the corresponding leveling off of the increase in the mean-square displacement, as shown in Fig. 6, provides a direct probe of this low-frequency elasticity. Physically, this leveling off corresponds to the maximum displacement of a droplet because of its thermal motion before it is trapped by the elasticity of the medium. Thus we suspect that this displacement is given roughly by equating the thermal energy per droplet to the elastic energy, or

$$\frac{k_B T}{a^3} \approx \frac{G' a^2}{\langle \Delta r_m^2 \rangle}, \quad (16)$$

where  $\langle \Delta r_m^2 \rangle$  is the maximum mean-square displacement measured from the light scattering. This approach provides a measure of the elastic modulus, as shown in Fig. 9, where we compare the values measured by light scattering, shown by the filled circles, with those measured by mechanical means, shown by the open squares. Very good agreement is obtained, confirming the validity of this technique. We note that the interpretation of the light-scattering data as a mean-square displacement of a single droplet becomes less well established as the volume fraction increases; nevertheless, good agreement with the mechanical data is obtained within this picture.

In addition to the low-frequency elasticity of the emulsion, the light-scattering data also provide a probe of the viscoelasticity at frequencies that are much higher than can be studied by traditional mechanical means, as can be observed clearly in Fig. 7 for  $\tilde{G}(s)$ . At the very highest frequencies the data must approach a linear behavior, reflecting fact that these emulsions are fluids; thus the viscosity is that of the solvent, corrected for the presence of the droplets. However, the most pronounced behavior at high frequencies is the  $s^{0.5}$  behavior observed on subtraction of the asymptotic limits.<sup>34</sup> This behavior is also observed for all the other volume fractions studied. The origin of this additional contribution to the modulus arises from the nature of the disordered packing of the droplets. As their volume fraction increases, the droplets deform to fit into the restricted volume, and this causes them to form flattened facets where two droplets are pressed together, leading to a repulsive force between the

centers of two neighboring droplets. However, for each droplet the forces that are due to all its neighbors must balance, so the net force on the droplet is zero. These interdroplet forces are only repulsive and act only between the centers of the drops. However, because of the disorder in the packing, there are bound to be some localized regions in which the droplets cannot elastically respond to a shear in some direction; instead the droplets can slide in this direction, thereby dissipating energy.<sup>33</sup> These regions are randomly situated and randomly oriented throughout the sample, and the response of these slip regions can be modeled<sup>34</sup> by analogy to the behavior of a random distribution of smectic layers.<sup>35</sup> The time response of these layers varies with the orientation of their slipping direction compared with the direction of the imposed shear, with the slowest response for those regions whose slip planes are nearly perpendicular to the direction of the shear, so the response is most nearly elastic. However, if the distribution of slip directions is random, the sum over directions yields a Gaussian form when all the contributions are included. This form leads directly to a term that varies as the square root of frequency and that contributes equally to both the real and the imaginary parts of the shear modulus.<sup>34</sup> Because some of the barriers to the slipping are sufficiently low, some regions will slip spontaneously owing to thermal excitations, leading to the observed  $s^{1/2}$  behavior in the data. Because those regions that slip do not support shear elastically, a weakening of the elastic or storage modulus of the emulsion results; indeed, the measured value of  $G'(\omega)$  is significantly lower than expected for these emulsions.<sup>32,33</sup> Inasmuch as this contribution arises from a viscous dissipation of a small volume, it is most readily apparent at high frequencies, where its contribution becomes greater than the purely elastic response of the rest of the emulsion. For this reason it cannot be seen with normal mechanical measurements; by contrast, the light-scattering method discussed here is ideally sensitive to this behavior.

Although the elasticity of the emulsions results from a fundamentally different origin, it is nevertheless quite similar to that of the hard spheres. In fact, although the characteristic values of the modulus differ by approximately seven decades, the contribution to the elasticity of the hard spheres is diverging as  $\phi_c$  is approached, whereas the contribution to the emulsions is decreasing. The two contributions must meet somewhere close to  $\phi_c$ . In fact, at the lowest volume fractions of the emulsions that were studied the data can be well interpreted in terms of the MCT, with parameters similar to those of the hard spheres near the glass transition. This is a consequence of the large Laplace pressure of the emulsion droplet; at lower volume fractions the osmotic pressure of the surrounding droplets is lower and cannot deform the shape of the droplet. Thus here the behavior of the emulsions should be identical to that of the hard spheres.

#### 4. CONCLUSIONS

The use of light scattering for measuring the viscoelasticity of complex fluids has several distinct advantages. Certainly the ability to measure mechanical properties of

complex fluids by using solely optical techniques can be of great use. In addition, the frequency range of this optical method is significantly greater than that of mechanical methods. Because the probe particle is so small, inertial effects do not limit the measurement until large frequencies. Thus the high-frequency response is limited by the ability to detect the initial decay of the correlation function. It is here that DWS can prove valuable, as it can probe motion over length scales that are significantly smaller than those of the traditional DLS and thus can be used to investigate dynamics at much higher frequencies. In addition, the use of DWS is of particular value and importance as the material becomes increasingly elastic, which leads to much more highly restricted motion, which cannot be detected with traditional DLS. However, although it is often quite convenient to use DWS, there is nothing intrinsic in this method that requires the exclusive use of DWS; instead, the choice of single or multiple light scattering is determined by the range over which the particle moves and thus by the elastic modulus, and by the nature of the sample and the degree of scattering that it exhibits. By varying the size of the scattering particle and by using both DLS and DWS, it should be possible to study materials with elastic moduli varying from  $\sim 10^{-2}$  to  $\sim 10^7$  dyn/cm<sup>2</sup>.

The frequency dependence of the rheological response of complex fluids often yields very valuable insight into their properties. Typical mechanical rheological measurements are limited in the range of frequencies to which they have access. A common way to overcome this limitation is through the use of time-temperature superposition, which exploits the temperature dependence of the characteristic time constants to shift their values relative to the experimentally accessible regime. By contrast, the extended range of frequencies that are accessible with the optical technique can be measured in a single experiment. Besides making the measurements more convenient, this method also eliminates the requirement of scaling with temperature and makes possible the study of materials whose rheological properties do not exhibit the time-temperature superposition.

Finally, an additional important feature of this technique is that it ensures that the equilibrium modulus is determined, as thermal excitations are responsible for the measurement technique. Indeed, this method can be viewed as the direct application of the fluctuation-dissipation theorem to measure the moduli; it is the response of the particle to a thermal fluctuation that is interpreted to yield the moduli of the medium. In addition, this method provides considerable new insight into the underlying origin of the viscoelasticity, as it directly relates the rheological response to the mean-square displacement of the scattering particles. Thus in this study the light-scattering results have provided new insight into the behavior of the hard spheres near the glass transition. The results were treated through the application of the mode-coupling theory to describe the viscoelasticity of hard-sphere colloidal glasses. In addition, the light-scattering results permitted us to measure the loss moduli of compressed emulsions at much higher frequencies, facilitating the direct observation of an unusual frequency dependence,  $\omega^{1/2}$ .

In this paper we have discussed an interpretation of dynamic light-scattering data that allows the frequency-dependent linear viscoelastic moduli of the surrounding media to be determined. We used the method to study the elasticity of concentrated suspensions of colloidal particles interacting as hard spheres and of compressed emulsions made from monodisperse droplets. Although the technique works very well for both of these samples, the theoretical basis of the interpretation is still completely phenomenological. As a result, further experimental tests of the applicability of this technique are clearly required. However, given the relative ease of making the measurements, the extended frequency range, and the new physical insight that it provides, this method is likely to find widespread use.

## REFERENCES

1. D. J. Pine, D. A. Weitz, P. M. Chaikin, and E. Herbolzheimer, "Diffusing wave spectroscopy," *Phys. Rev. Lett.* **60**, 1134-1137 (1988).
2. D. J. Pine, D. A. Weitz, J. X. Zhu, and E. Herbolzheimer, "Diffusing-wave spectroscopy: dynamic light scattering in the multiple scattering limit," *J. Phys. (Paris)* **51**, 2101-2111 (1990).
3. D. A. Weitz, D. J. Pine, P. N. Pusey, and R. J. A. Tough, "Nondiffusive Brownian motion studied by diffusing-wave spectroscopy," *Phys. Rev. Lett.* **63**, 1747-1750 (1989).
4. J. X. Zhu, D. J. Durian, J. Müller, D. A. Weitz, and D. J. Pine, "Scaling of transient hydrodynamic interactions in concentrated suspensions," *Phys. Rev. Lett.* **68**, 2559-2562 (1992).
5. T. G. Mason and D. A. Weitz, "Optical measurements of the linear viscoelastic moduli of complex fluids," *Phys. Rev. Lett.* **74**, 1250-1253 (1995).
6. A. J. C. Ladd, H. Gang, J. X. Zhu, and D. A. Weitz, "Time-dependent collective diffusion of colloidal particles," *Phys. Rev. Lett.* **74**, 318-321 (1995).
7. A. J. C. Ladd, H. Gang, J. X. Zhu, and D. A. Weitz, "Temporal and spatial dependence of hydrodynamic correlations: simulation and experiment," *Phys. Rev. E* **52**, 6550-6572 (1995).
8. B. J. Berne and R. Pecora, *Dynamic Light Scattering with Applications to Chemistry, Biology and Physics* (Wiley, New York, 1976).
9. J.-Z. Xue, D. J. Pine, S. T. Milner, X.-L. Wu, and P. M. Chaikin, "Nonergodicity and light scattering from polymer gels," *Phys. Rev. A* **46**, 6550-6560 (1992).
10. T. G. Mason, H. Gang, and D. A. Weitz, "Rheology of complex fluids measured by dynamic light scattering," *J. Mol. Struct.* (to be published).
11. P. M. Chaikin and T. Lubensky, *Principles of Condensed Matter Physics* (Cambridge U. Press, Cambridge, 1994).
12. W. B. Russel, D. A. Saville, and W. R. Schowalter, *Colloidal Dispersions* (Cambridge U. Press, Cambridge, 1989).
13. C. G. deKruif, J. W. Jansen, and A. Vrij, in *Complex and Supramolecular Fluids*, S. A. Safran and N. A. Clark, eds. (Wiley/Interscience, New York, 1987), p. 315.
14. T. Shikata and D. S. Pearson, "Viscoelastic behavior of concentrated spherical suspensions," *J. Rheol.* **38**, 601-611 (1994).
15. P. N. Pusey and W. van Meegen, *Nature (London)* **320**, 340-342 (1986).
16. P. N. Pusey and W. van Meegen, "Observation of a glass transition in suspensions of spherical colloidal particles," *Phys. Rev. Lett.* **59**, 2083-2086 (1987).
17. W. van Meegen and S. M. Underwood, "Glass transition in colloidal hard spheres: mode-coupling theory analysis," *Phys. Rev. Lett.* **70**, 2766-2769 (1993).
18. T. G. Mason and D. A. Weitz, "Linear viscoelasticity of colloidal hard spheres near the glass transition," *Phys. Rev. Lett.* **75**, 2770-2774 (1995).

19. P. N. Pusey and W. van Meegen, "Dynamic light scattering by non-ergodic media," *Physica A* **157**, 705–741 (1989).
20. D. A. Weitz, J. X. Zhu, D. J. Durian, H. Gang, and D. J. Pine, "Diffusing wave spectroscopy: the technique and some applications," *Phys. Scr.* **T49**, 610–621 (1993).
21. D. J. Durian, D. A. Weitz, and D. J. Pine, "Multiple light-scattering probes of foam structure and dynamics," *Science* **252**, 686–688 (1991).
22. W. van Meegen and S. M. Underwood, "Glass transition in colloidal hard spheres," *Phys. Rev. E* **49**, 4206–4216 (1994).
23. W. Götze and L. Sjogren, " $\beta$  Relaxation at the glass transition of hard-spherical colloids," *Phys. Rev. A* **43**, 5442–5452 (1991).
24. W. Götze and L. Sjogren, "Relaxation processes in supercooled liquids," *Rep. Prog. Phys.* **55**, 241–341 (1992).
25. I. M. de Schepper, H. E. Smorenburg, and E. G. D. Cohen, "Viscoelasticity in dense hard sphere colloids," *Phys. Rev. Lett.* **70**, 2178–2181 (1993).
26. R. A. Lionberger and W. B. Russel, "High frequency modulus of hard sphere colloids," *J. Rheol.* **38**, 1885–1895 (1994).
27. W. van Meegen and P. N. Pusey, "Dynamic light-scattering study of the glass transition in a colloidal suspension," *Phys. Rev. A* **43**, 5429–5441 (1991).
28. H. M. Princen, M. P. Aronson, and J. C. Moser, "Highly concentrated emulsions: film thickness and contact angle," *J. Colloid Interface Sci.* **75**, 246–250 (1980).
29. H. M. Princen and A. D. Kiss, "Static shear modulus," *J. Colloid Interface Sci.* **112**, 427–437 (1986).
30. J. Bibette, "Depletion interactions and fractionated crystallization for polydisperse emulsion purification," *J. Colloid Interface Sci.* **147**, 474–480 (1991).
31. T. G. Mason, A. H. Krall, H. Gang, J. Bibette, and D. A. Weitz, "Monodisperse emulsions: properties and uses," in *Encyclopedia of Emulsion Technology*, P. Becher, ed. (Dekker, New York, 1996), Vol. 4, pp. 299–335.
32. T. G. Mason, J. Bibette, and D. A. Weitz, "Elasticity of compressed emulsions," *Phys. Rev. Lett.* **75**, 2051–2054 (1995).
33. M.-D. Lacasse, G. Grest, D. Levine, T. G. Mason, and D. A. Weitz, "Model for the elasticity of compressed emulsions," *Phys. Rev. Lett.* **76**, 3448–3451 (1996).
34. A. J. Liu, S. Ramaswamy, T. G. Mason, H. Gang, and D. A. Weitz, "Anomalous viscous loss in emulsions," *Phys. Rev. Lett.* **76**, 3017–3020 (1995).
35. K. Kawasaki and A. Onuki, "Dynamics and rheology of diblock copolymers quashed into microphase-separated states," *Phys. Rev. A* **42**, 3664–3667 (1990).